Graduate School of Pure and Applied Sciences

Alloy design and texture control of metastable β-Ti alloys with low modulus and high strength
(低弾性率と高強度を備えた準安定 β-Ti 合金の合金設計と集合組織制御)

KIM, KYONG MIN

Doctoral Program in Materials Science
201630126
Doctor of Philosophy in Engineering
Advised by KIM, HEE YOUNG

1. Introduction

Metallic materials such as stainless steels, cobalt-chromium based alloys and Ti alloys have been extensively used as structural biomaterial. One of the critical issues associated with metallic biomaterials is their high Young's modulus because the mismatch of the elastic modulus between metallic implants and adjacent bone tissues can lead to stress shielding, causing bone resorption and osteoporosis [1,2]. Among metallic biomaterials, Ti and its alloys have explicitly received more attention due to not only their balanced combination of excellent mechanical properties and biocompatibility, but also relatively lower Young's modulus than stainless steels and cobalt-chromium based alloys [3-5]. However, when compared with Young's modulus of bone tissues (10-30 GPa), commercially pure Ti (CP-Ti) and Ti–6Al–4V, which are the most commonly used Ti based alloys for biomedical applications, possess a considerably higher Young's modulus about 110 GPa.

Over the last decades, there have been significant efforts to develop Ti alloys that have Young's modulus much closer to those of bone tissues [6-12]. Ti alloys have two stable phases, α phase with a hexagonal close-packed (hcp) crystal structure and β phase with a body centered cubic (bcc) structure and they are classified into three main categories according to major constituent phases: α-type, (α+β)-type, and β-type Ti alloys. Among them β-type Ti alloys have been confirmed to have the lowest Young's modulus; thus they have attracted increasing research attention in recent years. Up to date, many β-type Ti alloys have been developed, such as Gum metal, Ti–Nb–Ta–Zr, Ti–Nb–Sn, Ti–Nb–Zr, Ti–Nb–Hf and Ti–Nb–Zr–Sn. It is noted that most of β-type Ti alloys exhibiting low Young's modulus contain Nb as a β stabilizing alloying element due to the moderate β phase stabilizing ability and biocompatibility.

It has also been confirmed that Young's modulus of β-type Ti alloys is strongly dependent on the stability of the β phase [6, 9, 20]. Generally, Young's modulus decreases as the β phase becomes unstable; however the decrease in the stability of the β phase stimulates the formation of α" martensite phase and ω phase, leading to the increase in Young's modulus. In order to assess the stability of the β phase and to optimize the alloy composition, various approaches have been proposed, including Mo equivalent (Moeq), electron to

atom ratio (e/a), and d-electron alloy design theory. The Mo equivalent is an empirical parameter representing the contribution of alloying elements on the stability of β phase in comparison to that of Mo. Although Moeq has been widely used as a guideline to design of β-type Ti alloys, there have been some controversial issues on the effect of alloying elements on the stability of β phase and modification has been continued. The average number of valence electrons per atom or electron to atom ratio (e/a) is also a representative measure of the elastic constants of bcc crystals. It has been reported that as a decrease in the value of e/a, the shear modulus $c'=(c_{11}-c_{12})/2$ and bulk modulus B of a bcc crystal decrease, causing the β phase to become unstable [6, 9, 12]. The d-electron alloy design theory is based on molecular orbital calculations. Two key parameters of this theory are the bond order (Bo) and the d-orbital energy level (Md) which are calculated for each alloying element. Bo is parameter to show the overlapping of the electron clouds of adjacent two atoms, which is a measure of the covalent bond strength between Ti and alloying element. Md correlates with electronegativity and atomic radius of each alloying element. The average values of Bo and Md, calculated by taking the compositional averages, have been utilized to predict phase boundaries and the stability of the β phase. Experimental results have validated that the β phase becomes unstable with decreasing Bo or with increasing Md [13, 14]. However, it has been pointed out that the phase boundary line in the Bo-Md map shifts as the change of constituent alloying elements.

β-type Ti alloys have also attracted attention as biomedical shape memory alloys [15, 16]. The phase stability of the β phase is a key factor governing shape memory effect and superelasticity in β-type Ti alloys because they are related to martensitic transformation from the β phase to the orthorhombic α" martensite phase. It has been also reported that the Bo-Md map for Ti alloys is useful to predict the martensitic transformation temperature and deformation mechanism. Despite such extensive research, much uncertainty still exists on the relations among Young's modulus, martensitic transformation behavior and the values of e/a, Bo and Md, and the experimental data are still insufficient to understand the mechanisms involved.

β-type Ti alloys are typically prepared by casting followed by hot working and/or cold working and heat treatment and these processes develop strong crystallographic texture. Young's modulus is strongly dependent on the crystal orientation; therefore the texture is an important parameter in determining Young's modulus. Young's moduli in the <100> direction E_{100} is approximately two times lower than Young's modulus in the <111> direction E_{111}. Generally the recrystallization texture is affected by not only deformation condition but also heat treatment condition. Also it is expected that the stability of β-alloys affects the deformation mechanism and texture development.

Thus, the purpose of this research is ultimately to assist in the design of promising new biomaterials for implant applications, with a particular focus on microstructural control. As such, the primary aims of this research can be summarized as follows;

- ✓ Clarification on the relation between DV-Xα, e/a ratio theory and experimental results in designing of β-Ti alloys
- ✓ Optimization of composition and thermomechanical processing parameter

This study focuses on the effect of the Zr addition on the phase stability and Young's modulus in Ti–Nb alloys. Ti–Nb–Zr alloys with various Nb and Zr contents were fabricated and the composition dependence of

phase constitution and deformation behavior was investigated. The phase boundary between the β phase and the α" martensite phase in Ti–Nb–Zr alloys was clarified. The relations among phase stability, martensitic transformation behavior and Young's modulus were analyzed. Finally, a novel guideline to design β-type Ti alloys with low Young's modulus was proposed.

2. Experimental procedure

Ti-Nb-(0-18)Zr and Ti-Zr-Nb-Sn-(1-3)Mo alloys (at%; all percentage in this study denote atomic percent unless indicated otherwise) ingots were casted by Ar arc melting. The ingots were flipped and re-melted six times to improve their homogeneity. The change in weight caused by arc melting was less than 0.05 weight% and was judged to be negligible, requiring no chemical analysis. The ingots were homogenized at 1273 K for 7.2 ks, and solution-treated at 1273 K for 3.6 ks in vacuum, followed by water quenching. Then the ingots were cold-rolled into plates of approximately 0.15 mm in thickness with a final reduction ratio of 98.5%. An electrical discharge machine was used to cut specimens for mechanical test and microstructure analysis. The specimens were chemically etched to remove surface damage. The specimens were encapsulated in quartz tube in an Ar atmosphere and annealed at 1173 K for 0.3 ks, followed by water quenching. The oxidized surface that was generated during quenching was removed by chemical etching. The constituent phases were characterized by X-ray diffraction (XRD) with Cu K_α radiation (40 kV, 30 mA) in the 2θ range from 20° to 90° at room temperature. The textures of the as-rolled and annealed specimens were investigated by taking pole figures from three crystal planes, i.e. {110}, {200} and {211} of the β phase, and orientation distribution functions (ODF) were derived using the three pole figures. Tensile tests along the rolling direction using dog-bone specimens with a 20 mm gauge length and 1.5 mm width were carried out at a strain rate of 0.005 mm/s at room temperature. Microstructural characterization was made by electron backscattered diffraction (EBSD). Specimens for EBSD observations were prepared by electrolytic polishing at 233 K perchloric acid (60%), 1-butanol, and methanol (1:6:10).

3. Results and Discussion

3.1 The effect of Zr addition in Ti-Nb alloys

3.1.1 Microstructure of Ti-Nb-Zr alloys

Phase constitutions of (a) Ti-Nb, (b) Ti-Nb-4Zr, (c) Ti-Nb-8Zr, (d) Ti-Nb-12Zr, and (e) Ti-Nb-18Zr alloys annealed at 1173 K for 0.3 ks were investigated by XRD and the results are shown in Fig. 1. It is seen that the phase constitution of the annealed alloys in each Zr contents is influenced by the content of Nb. The peaks from both α" and β were observed in the alloys with lower Nb contents, such as 24Nb, 25Nb, 21Nb-4Zr, 18Nb-8Zr, 16Nb-12Zr, and 13Nb-18Zr. Even though the intensity of peak was weak (2theta = 65 degree), Ti-19Nb-8Zr and Ti-17Nb-12Zr was also observed the peak of α" phase. On

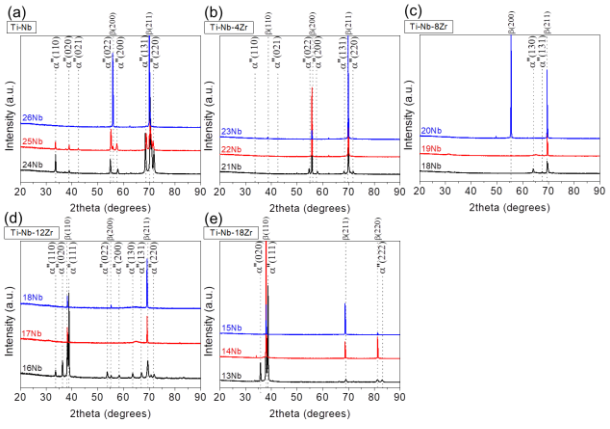

Fig. 1 X-ray diffraction patterns of Ti-Nb-Zr alloys annealed at 1173 K for 0.3 ks.

the other hand, the diffractions of the other alloys with higher Nb contents exhibit β phase only. These results are consistent with the previous report that Nb and Zr decreased Ms temperature in Ti-Nb-Zr alloys.

3.1.2 Stress-strain curves of Ti-Nb-Zr alloys

Fig. 2 shows the tensile stress-strain curves of (a) Ti-Nb, (b) Ti-Nb-4Zr, (c) Ti-Nb-8Zr, (d) Ti-Nb-12Zr, and (e) Ti-Nb-18Zr alloys annealed at 1173 K for 0.3 ks, respectively. All specimens exhibited a double yielding behavior, which is related to stress-induced martensitic transformation for the first yielding and dislocation slip for the second yielding, as shown by arrows. The first and second yield stresses indicated by black and grey arrows was measured by an intersection of elastic deformation line with the extended plateau, respectively. The critical stress for the first and second yielding significantly changed depending on Nb and Zr contents. On the other hand, the ultimate tensile strength gradually increased with increase of Zr contents, which is attributed to the solid-solution strengthening.

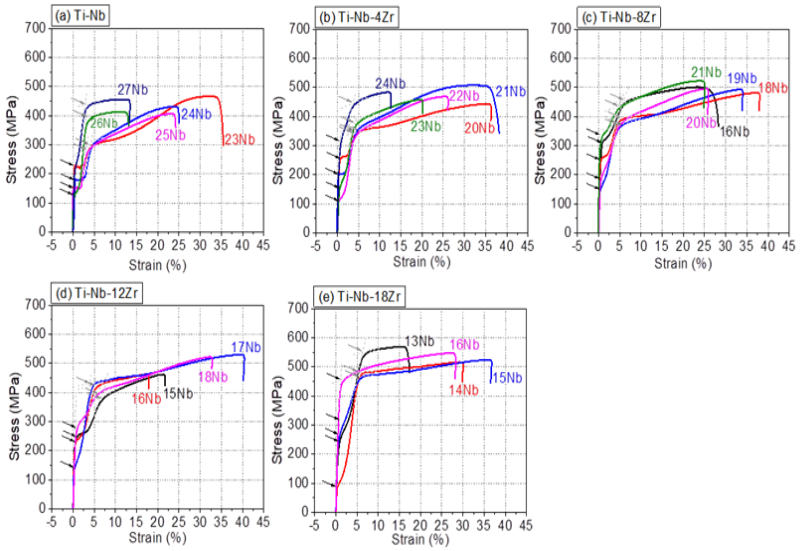

Fig. 2. Stress-strain curves obtained at room temperatures for the Ti-Nb-Zr alloys.

3.1.3 Young's modulus and yield strength

Fig. 3 shows the variation of Young's modulus (Fig. 3(a)), and the relationship between Young's modulus and first yield strength (Fig. 3(b)) that was measured from Fig. 3, as a function of Nb contents in Ti-Nb, Ti-Nb-4Zr, Ti-Nb-8Zr, Ti-Nb-12Zr, and (e) Ti-Nb-18Zr alloys. It is seen that, for the binary Ti-Nb and ternary Ti-Nb-Zr alloys, Young's modulus gradually decreased with decrease of Nb contents reaching a minimum point, and then Young's modulus increased with further decreasing Nb content. The increase in Young's modulus in alloys with lower Nb content is supposed to be due to the formation of α" martensite. Also it is noticed that the minimum Young's modulus gradually decreases with

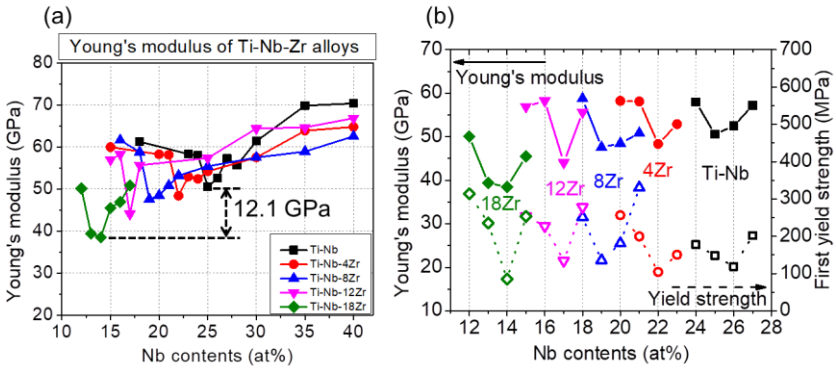

Fig. 3. Plots of variation of Young's modulus (a), and relationship between Young's modulus and first yield strength (b).

increasing Zr content, i.e. from 50.6 GPa in Ti-25Nb to 38.5 GPa in Ti-14Nb-18Zr. In addition, it is seen in Fig. 3 (b) that both Young's modulus and yield strength show a very similar V-shaped tendency with respect to the Nb content. For example, the lowest Young's modulus (38.5 GPa) was measured in the Ti-14Nb-18Zr alloy, which also exhibits the lowest yield strength (85.5 MPa).

Previous studies have demonstrated that e/a is a dominant factor governing the elastic constants and Young's modulus of bcc transition metals including β-type Ti alloys. In order to understand the effect of Zr content on the lowest Young's modulus for each series of alloys with different Zr content, the Young's moduli of the Ti–25Nb, Ti–22Nb–4Zr, Ti–19Nb–8Zr, Ti–17Nb–12Zr and Ti–14Nb–18Zr alloys are plotted in Figure 4 as a function of e/a. For comparison purposes, the results of some β-type Ti alloys developed for low Young's modulus alloys are included in Figure 4. Note that e/a of the alloys investigated in this study decreased with increasing Zr content as follows: Ti–25Nb, 4.25; Ti–22Nb–4Zr, 4.22; Ti–19Nb–8Zr, 4.19; Ti–17Nb–12Zr, 4.17; and Ti–14Nb–18Zr, 4.14. The decrease is attributed to the fact that Zr decreases Ms of the alloys, and the addition of Zr shifts the phase boundary of (β+α")/β toward lower Nb content. Although the data were somewhat scattered, there is a clear tendency of decreasing Young's modulus with decreasing e/a in accordance with the previous reports. As a result, it is suggested that Zr is an effective alloying element in reducing Young's modulus because it decreases the lower limit of e/a to maintain the β phase. Similarly, Sn is considered as a useful alloying element because it also decreases Ms of the alloys while keeping e/a. These results may have important implications for developing useful guidelines for alloy design.

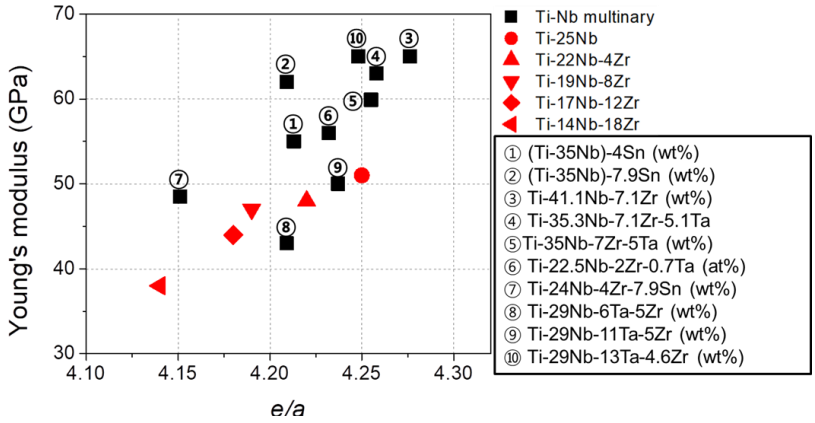

Fig. 4. Comparison of Young's modulus of the Ti–Nb based alloys as a function of e/a.

3.2 The addition of Sn and Mo in Ti-Zr-Nb alloys

As noted above, the addition of Zr in Ti-Nb alloys has led to decrease of Young's modulus as well as martensitic transformation. However, mechanical strength is still low when compared with used biomaterials. Phase diagrams of the binary Ti-Nb and Ti-Mo systems show that Mo has a stronger β-stabilizer. Moreover, the atomic radius of Ti, Nb, and Mo are known to be 146m 147 and 140 pm, respectively, from which the solid solution hardening effect of Mo is expected to be higher when Mo was substituted for Nb. And the addition of Sn, which is considered as a neutral element like Zr, decreases the transformation temperature. Moreover the addition of Sn is expected to reduce the Young's modulus of the alloy by suppressing ω phase formation.

3.2.1 Microstructure of Ti-Zr-Nb-Sn-(1-3)Mo alloys

The XRD profiles of Ti-Zr-Nb-Sn-(1-3)Mo alloys (a) as-rolled and (b) annealed at 1173 K for 0.3 ks are shown in Fig. 5, respectively. It is noted that each peak of the as-rolled specimens is broader than that of annealed specimens. This is due to the residual stress which was introduced during cold-rolling. The different peaks for annealed specimens were observed with different Mo contents. The apparent α" martensite phase was observed at a Mo content 1.0 at%, indicating that the martensitic transformation finish temperature of the alloys are higher than room temperature. And the β parent phase appeared when the Mo content was 2-3 at%, indicating that the increase in Mo content stabilized the β parent phase. The annealed 2.0Mo alloy is composed of a β single phase, while two phases of β and α" martensite are clearly seen after cold-rolling. This observation indicates that stress-induced martensitic transformation occurs by cold rolling in the 2.0Mo alloy.

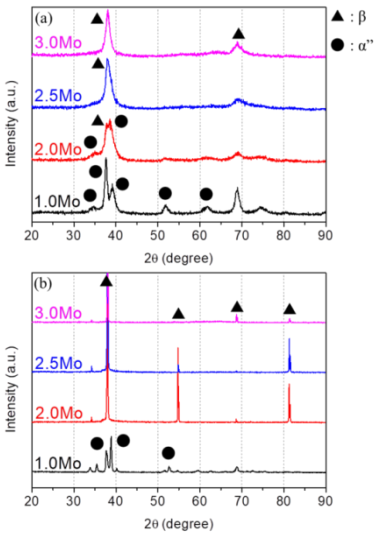

Fig. 5. X-ray diffraction patterns of Ti-Zr-Nb-Sn-(1-3)Mo alloys annealed at 1173 K for 0.3 ks.

Fig. 6 shows EBSD inverse pole figures maps of rolling direction of annealed Ti-Zr-Nb-Sn-(1-3)Mo alloys. The 1.0Mo alloy is mostly composed of typical lath-shaped or fine acicular martensitic α" phase and a little β phase (black phase). On the other hand, only equiaxed β grains can be observed with similar grain size of about 40 μm in the 2.0Mo, 2.5Mo and 3.0Mo alloys. The microstructural observations are consistent with the XRD results in Fig. 6. It is also noted that the addition of Mo led to change the recrystallization texture. This is because the deformation mechanisms of titanium alloys are strongly depends on chemical composition, which change from martensite transformation, to mechanical twinning and eventually, dislocation slip with an increase in the β phase stability. Thus, it can be deduced that the variation of deformation mechanisms by Mo addition led to change of recrystallization texture. However, the formation mechanism of recrystallization is still not clear.

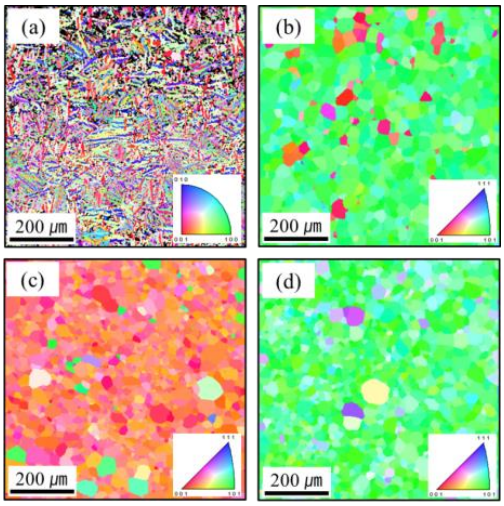

Fig. 6. EBSD inverse pole figure maps of rolling direction of annealed alloys: (a)1.0Mo, (b)2.0Mo, (c)2.5Mo, and (d)3.0Mo alloys.

3.2.2 Mechanical properties of Ti-Zr-Nb-Sn-(1-3)Mo alloys

Fig. 7 shows the tensile stress-strain curves of the Ti-Zr-Nb-Sn-(1-3)Mo alloys obtained at room temperature. The mechanical properties including Young's modulus (E), ultimate tensile strength (UTS), and elongation (δ) are measured using the tensile stress-strain curves in Fig. 8, and the results are summarized in Table 1. It is clearly seen that not only the first yielding stress but also the secondary yielding stress increases with increasing Mo content, where the first yielding corresponds to stress induced martensitic transformation

and the second yielding is due to the plastic deformation. The various stages of 1.0Mo alloy are identified as the initial elastic deformation, stress plateau associated with variant reorientation, elastic deformation of oriented martensite, and elastic/plastic deformation of oriented martensite. The large elongation of 21.8% in the 2.0Mo alloy was observed due to the twinning induced plasticity effect. It is also interesting to note that the 2.5Mo alloy exhibited the lower Young's modulus compared to 2.0Mo alloy, although the β-phase is more stable. The details about this will be discussed next chapter.

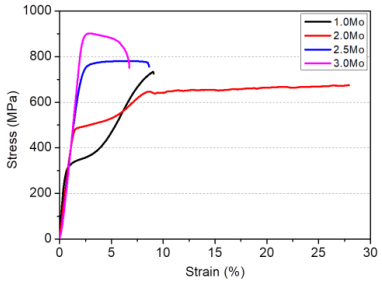

Fig. 7. Stress-strain curves obtained from tensile tests of Ti-Zr-Nb-Sn-(1-3)Mo alloys annealed

Table 1. Mechanical properties of Ti-Zr-Nb-Sn-(1-3)Mo alloys including Young's modulus (E), ultimate tensile strength (UTS), and elongation (δ).

	E (GPa)	UTS (MPa)	δ (%)
1.0Mo	58.5	733	9.0
2.0Mo	44.0	674	21.8
2.5Mo	40.4	767	8.6
3.0Mo	47.0	900	6.7

3.2.3 Texture and Young's modulus of Ti-Zr-Nb-Sn-(2-3)Mo alloys

Fig. 8 shows φ_2=45° sections of ODFs of Ti-Zr-Nb-Sn-(2-3)Mo alloys as-rolled and annealed at 1173 K for 0.3 ks, and Fig. 9 shows a schematic of ODF section at φ_2=45° in bcc metals. Deformation and recrystallization texture exhibited dependence of Mo content. For deformation texture, γ-fiber texture developed with increase of Mo contents. For annealed specimens, the strong {001}<011> rotated cube texture was observed in the 2.0Mo alloys. It has been well documented that {hkl}β<110>β type texture is favorable for a large recovery strain in superelastic Ti alloys because <110>β directions exhibits the largest transformation strain among all the crystallographic directions, while the 2.5Mo alloy showed strong {011}<001> Goss type texture. And the 3.0Mo alloy showed γ-fiber texture (normal direction (ND)//<111>). Inverse pole figures for RD shown in Fig. 10 indicate different intensity distribution in the alloys: <011> direction of crystals aligns parallel to RD in the 2.0Mo and 3.0Mo alloys, while in the 2.5Mo alloy the intensity of <001> becomes dominant. The Young's modulus of 2.0Mo, 2.5Mo, and 3.0Mo alloys

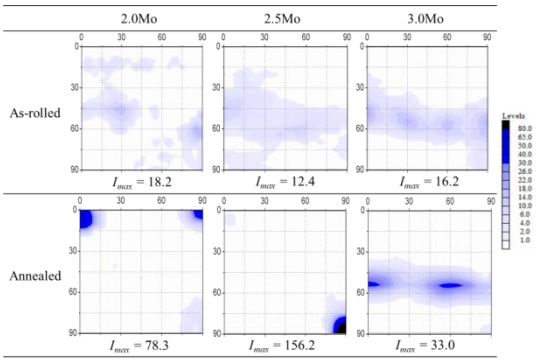

Fig. 8 Sections (φ_2=45°) of ODFs of the Ti-Zr-Nb-Sn-(2-3)Mo alloys as-rolled and annealed.

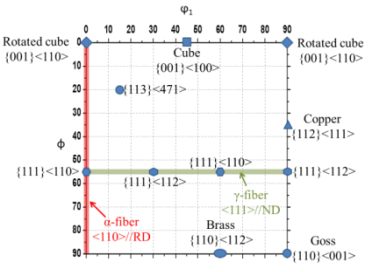

Fig. 9. Schematic illustration of the important texture components in bcc materials.

are measured to be 44.0 GPa, 40.4 GPa, and 47.0 GPa, respectively. As is known, for β-Ti alloys, a high content of β-stabilizing elements leads to high Young's modulus; however the 2.5Mo alloy exhibited lower Young's modulus compared with 2.0Mo alloy. This is due to the formation of strong Goss texture, which is favorable for lower Young's modulus among the crystallographic orientations.

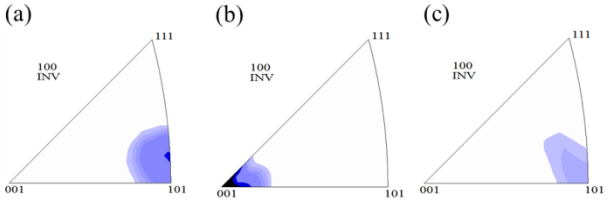

Fig. 10. Inverse pole figure maps for rolling direction of (a) 2.0Mo, (b) 2.5Mo, and (c) 3.0Mo alloy.

3.2.4 Texture evolution depending on cold-rolling ratio

In order to investigate the texture evolution depending on cold-rolling ratio and annealing time for 2.0Mo (Rotated cube) and 2.5Mo (Goss) alloys. Fig. 11 shows the XRD profiles of the as-rolled specimens of (a) 2.0Mo alloy, (b) 2.5Mo alloy and annealed at 1173 K for 0.3 ks of (c) 2.0Mo alloy, and (d) 2.5Mo alloy, respectively. As mentioned in chapter 3.2.1, the 2.0Mo alloy exhibited two phases of β and α" martensite are clearly seen after cold-rolling. The intensity of α" martensite phase became strong with increase of cold-rolling ratio, while β-phase was only detected in the 2.5Mo alloy. For annealed specimens, both 2.0Mo and 2.5Mo alloys showed only β-phase although the relative intensity of peaks changed with cold-rolling ratio.

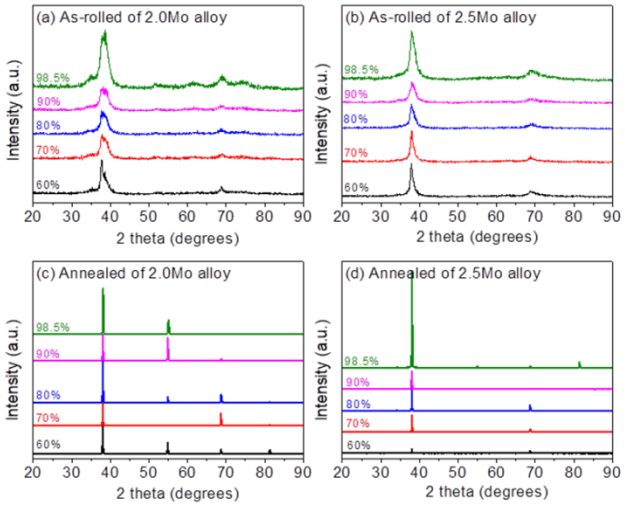

Fig.11. XRD profiles of as-rolled and annealed specimens.

Fig. 12 and 13 shows the as-rolled and annealed ODF maps of the 2.0Mo and 2.5Mo alloys, respectively. For as-rolled of 2.0Mo alloy, γ-fiber developed with increase of cold-rolling to 90% of cold rolling ratio. The γ-fiber disappeared after further cold-rolling in 98.5%. For annealed 2.0Mo alloy, texture development was negligible to 70% of rolling ratio, although the maximum intensity slightly increased. A weak {001}<110> texture developed in 80% and sharpened dramatically for 90%. This is because the number of recrystallization

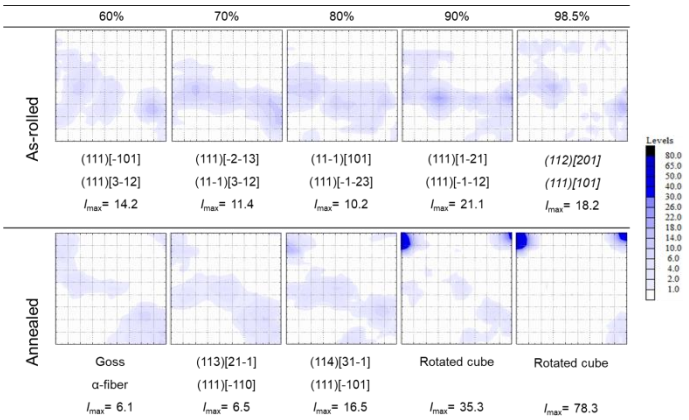

Fig. 12. ODF maps of as-rolled and annealed 2.0Mo alloy with different cold-rolling ratio.

initiation sites was increased by increasing rolling ratio.

For as-rolled 2.5Mo alloy as shown in Fig. 13, γ-fiber developed regardless of cold-rolling ratio. This γ-fiber develop under the activation of {110} and {112} slip systems in bcc metals by relaxed Taylor model. For annealed 2.5Mo alloy, texture development was slowly below 90% ratio, and a weak {001}<110> texture developed in 90% ratio. A very strong {001}<110> texture was observed in the specimen cold rolled with a reduction up to 98.5%. This results indicate that a fully recrystallized {001}<110> texture, which is desirable for the implant use, is achieved by controlling chemical composition, deformation condition, and heat treatment condition.

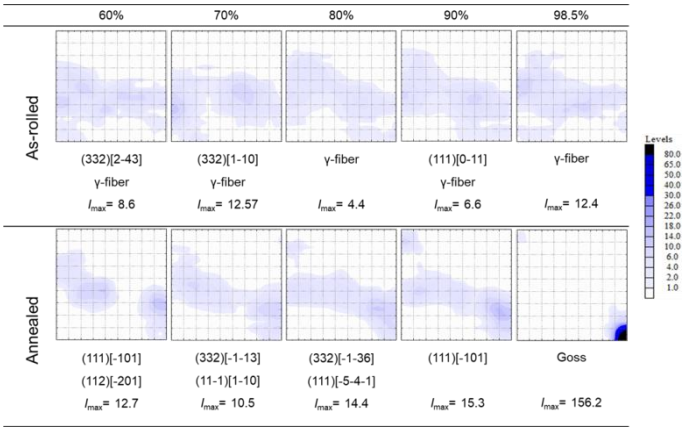

Fig. 13. ODF maps of as-rolled and annealed 2.5Mo alloy with different cold-rolling ratio.

4. Conclusions

In the present study, the effect of alloying elements on mechanical properties and microstructure evolution of Ti-based alloys has been studied. The major results of this research can be summarized as follows:

(1) The effects of the Nb and Zr contents on phase constitution, transformation temperature, deformation behavior and Young's modulus in Ti–(12-40)Nb–(0-18)Zr alloys were investigated. Young's modulus gradually decreases with decreasing Nb content, reaching a minimum value and then increases again with further decreasing Nb content. The Nb content taking the minimum value of Young's modulus was shifted to lower values as the increase in the Zr content. The Ti–25Nb, Ti–22Nb–4Zr, Ti–19Nb–8Zr, Ti–17Nb–12Zr and Ti–14Nb–18Zr alloys exhibit the lowest Young's moduli among Ti–Nb–Zr alloys with Zr contents of 0, 4, 8, 12, and 18 at.%, respectively. The minimum Young's modulus decreases with increasing Zr content. Particularly, the Ti–14Nb–18Zr alloy exhibits a very low value of 39 GPa.

(2) In order to improve the mechanical strength of Ti-Zr-Nb, the Ti-Zr-Nb-Sn-(1-3)Mo alloys were designed. The apparent α" martensite phase was observed at a Mo content of 1.0 at%, and the β parent phase appeared when the Mo content was 2~3 at%. Thus, the increase in Mo content stabilized the β parent phase.

(3) Different mechanical behavior was observed depending on Mo contents. The 1.0Mo and 2.0Mo alloys exhibited two-stage yielding, which is similar to that occurs in many shape memory alloys and superelastic alloys. The 2.5Mo and 3.0Mo alloys showed a single-stage yielding, indicating that the stress for inducing martensite is higher than that of the slip deformation due to dislocations.

(4) Recrystallization texture also exhibited strong composition dependence. The 2.0Mo alloy showed {001}<110> type texture, while 2.5Mo alloy presented {110}<001> type Goss texture. And 3.0Mo alloy showed γ-fiber texture. Inverse pole figures for RD indicate different intensity distribution in the alloys: <011>β direction of crystals aligns parallel to RD preferentially in the 2.0Mo and 3.0Mo alloy, while in the

2.5Mo alloy the intensity of <001> becomes dominant. 2.5Mo alloy exhibited the lowest Young's modulus compared with 2.0Mo and 3.0Mo alloys. This is due to the formation of strong Goss texture, which is favorable for lower Young's modulus among the crystallographic orientations.

(5) The Ti-Zr-Nb-Sn-2.5Mo alloy exhibited an excellent combination of ultralow Young's modulus and high strength as can be confirmed by comparison with other alloys from literature survey in Fig. 14.

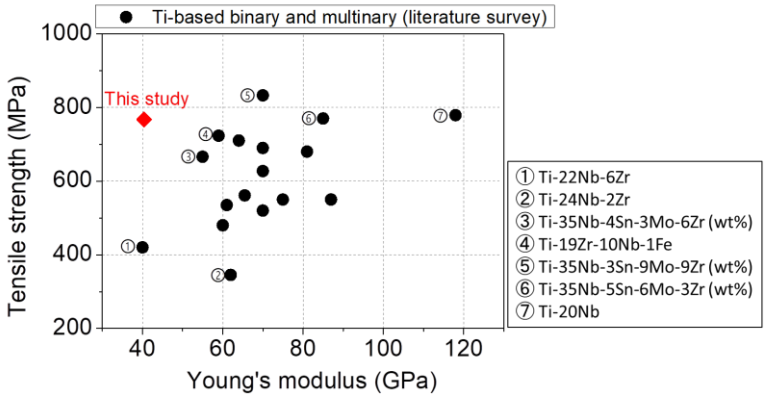

Fig. 14. Comparison of Young's modulus and strength between the Ti-Zr-Nb-Sn-2.5Mo alloy and the alloys from literature survey

References

1. Niinomi, M.; Nakai, M.; Hieda, J. Development of new metallic alloys for biomedical applications. Acta Biomater. 2012, 8, 3888-3903.

2. Chen, Q.; Thouas, G.A. Metallic implant biomaterials. Mater. Sci. Eng. R. 2015, 87, 1-57.

3. Geetha, M.; Singh, A.K.; Asokamani, R.; Gogia, A.K. Ti based biomaterials, the ultimate choice for orthopaedic implants - A review, Prog. Mater. Sci. 2009, 54, 397-425.

4. Li, Y.; Yang, C.; Zhao, H.; Qu, S.; Li, X.; Li, Y. New Developments of Ti-Based Alloys for Biomedical Applications. Materials 2014, 7, 1709-1800.

5. Niinomi, M. Mechanical biocompatibilities of titanium alloys for biomedical applications. J. Mech. Behav. Biomed. Mater. 2008, 1, 30-42.

6. Ozaki, T., Matsumoto, H., Watanabe, S.; Hanada, S. Beta Ti alloys with low Young's modulus. Mater. Trans. 2004, 45, 2776-2779.

7. Laheurte, P.; Prima, F.; Eberhardt, A.; Gloriant, T.; Wary, M.; Patoor, E. Mechanical properties of low modulus β titanium alloys designed from the electronic approach. J. Mech. Behav. Biomed. Mater. 2010, 3, 565–573.

8. Zhao, X.; Niinomi, M.; Nakai, M.; Ishimoto, T.; Nakano, T. Development of high Zr-containing Ti-based alloys with low Young's modulus for use in removable implants. Mater. Sci. Eng. C. 2011, 31, 1436-1444.

9. You, L.; Song, X. A study of low Young's modulus Ti-Nb-Zr alloys using d electrons alloy theory. Scripta Mater. 2012, 67, 57-60.

10. Hao. Y.L.; Li. S.J.; Sun. S.Y.; Yang. R. Effect of Zr and Sn on Young's modulus and superelasticity of Ti-Nb-based alloys. Mater. Sci. Eng. A 2006, 441, 112-118.

11. Hao. Y.L.; Li. S.J.; Sun. S.Y.; Zheng, C.Y.; Yang. R. Elastic deformation behavior of Ti–24Nb–4Zr–7.9Sn for biomedical applications. Acta Biomater. 2007, 3, 277–286.

12. Tane, M.; Akita, S.; Nakano, T.; Hagihara, K.; Umakoshi, Y.; Niinomi, M.; Nakajima, H. Peculiar elastic behavior of Ti–Nb–Ta–Zr single crystals. Acta Mater. 2008, 56, 2856–2863.

13. Abdel-hady, M.; Hinoshita, K.; Morinaga, M. General approach to phase stability and elastic properties of β-type Ti-alloys using electronic parameters. Scripta Mater. 2006, 55, 477-480.

14. Abdel-hady, M.; Fuwa, H.; Hinoshita, K.; Kimura, H.; Shinzato, Y.; Morinaga, M. Phase stability change with Zr content in β-type Ti-Nb alloys. Scripta Mater. 2007, 57, 1000-1003.

15. Kim, H.Y.; Ikehara, Y.; Kim, J.I.; Hosoda, H.; Miyazaki, S. Martensitic transformation, shape memory effect and superelasticity of Ti–Nb binary alloys. Acta Mater. 2006, 54, 2419-2429.

16. Fu, J.; Yamamoto, A.; Kim, H.Y.; Hosoda, H.; Miyazaki, S. Novel Ti-base superelastic allys with large recovery strain and excellent biocompatibility. Acta Biomater. 2015, 17, 56-67.